Combustion and Flame xxx (xxxx) xxx

Contents lists available at ScienceDirect

Combustion and Flame

journal homepage: www.elsevier.com/locate/combustflame

Theoretical studies of real-fluid oxidation of hydrogen under supercritical conditions by using the virial equation of state

Junfeng Bai[a,b,c], Peng Zhang[c], Chong-Wen Zhou[b,*], Hao Zhao[a,*]

[a] College of Engineering, Peking University, Beijing 100871, China
[b] School of Energy and Power Engineering, Beihang University, Beijing 100191, PR China
[c] Department of Mechanical Engineering, The Hong Kong Polytechnic University, Kowloon, Hong Kong

ARTICLE INFO

Article history:
Received 1 October 2021
Revised 8 December 2021
Accepted 14 December 2021
Available online xxx

Keywords:
Real fluid
Thermodynamics
Virial equation of state
Hydrogen
Supercritical modelling

ABSTRACT

The Virial equation of state (EoS) was employed to describe the real-fluid impact on H_2 oxidation simulation. Different from conventional empirical EoS methods fitted by using critical pressures and temperatures, such as Redlich-Kwong (RK) EoS, the Virial method was constructed with including intermolecular interactions, potentials, and molecular polarizations coupled with real-fluid partition function theory in this work. The Virial method was for the first time incorporated into Cantera software to realize real-fluid simulations with deeper-level physical insights. A series adiabatic/isothermal flow reactor and ignition delay simulations in H_2O, N_2, and CO_2 diluents were performed. The calculations of species compressibility factors and thermodynamic properties by using the Virial method showed a better agreement with experimental data in literature than using the RK method. The Virial method also possessed a better performance in predicting experimental H_2 ignition delay times and H_2 speciation profiles from literatures. The effects of real fluid through corrections of compressibility factors, thermodynamic properties, and chemical potentials on supercritical H_2 oxidation simulations in H_2O diluents have been rigorously analyzed, respectively. Moreover, the Virial method performed well at adiabatic conditions in the bath gas of polar molecules like H_2O, due to its consideration of molecular polarizations and higher accuracy of thermodynamic property calculations. We believed the Virial method could not only provide accurate estimations of real-fluid behavior, but also provided physical insights in the intermolecular interactions under supercritical conditions.

1. Introduction

In advanced engines and gas turbines, supercritical combustion (100–300 atm) has great potential due to its high combustion efficiency, ultra-lean fuel flammability, and low emissions [1–6]. However, under supercritical conditions, the intermolecular attraction cannot be ignored, while new physical mechanisms might be important in thermodynamics, transport, and reaction kinetics [7]. Therefore, theoretical investigations of real-fluid impact on supercritical combustion are highly needed to predict behavior of fluids in computational fluid dynamics and combustion modeling [8,9]. Especially, the construction and utilization of the real-fluid equation of state (EoS) is crucial for the theory development.

Scott and van Konynenburg [10] proposed the famous van der Waals semi-quantitative EoS for describing the real-fluid behavior:

$$\left(p+\frac{a}{\tilde{V}^2}\right)\left(\tilde{V}-b\right)=RT \tag{1}$$

where $\tilde{V}$. is volume per mole, the constant a is a measure of intermolecular interaction and constant b represents the volume of molecules. Subsequently, Pitzer and Curl [11,12], MacDougall [13], Beattie and Bridgeman [14], and Benedict et al. [15] reported a series of empirical EoS. Thmost widely used empirical EoS is Redlich-Kwong (RK) EoS and its modified forms, Soave-Redlich-Kwong (SRK) [16] and Peng-Robinson (PR) [17] EoSs. Subsequently, Kogekar et al. [18] simulated real-fluid oxidation of n-dodecane/O_2/N_2 mixtures using the RK method in Cantera program [19]. They also provided the calculation method of RK, thermodynamic properties, and chemical potentials in the code. Liang et al. [4] compared real-fluid effects in laminar flame simulations of supercritical hydrogen/air and methane/air mixtures using Van der Waals EoS, RK EoS and SRK EoS, respectively, in Chemkin II program. However, they did not consider the real-fluid effects involving chemical potentials. Li et al. [20] incorporated real-fluid behaviors into hydrogen oxidation simulations in supercritical $H_2/H_2O/CO_2$ mixtures

* Corresponding authors.
E-mail addresses: h.zhao@pku.edu.cn (H. Zhao), cwzhou@buaa.edu.cn (C.-W. Zhou).

https://doi.org/10.1016/j.combustflame.2021.111945
0010-2180/

using PR EoS. Unfortunately, the empirical EoS methods in literatures are constructed based on limited high pressure experimental data, while lack of physical insights in molecular interactions and intermolecular potentials. As such, the real-fluid effect on substance property, thermodynamic property, and chemical potentials has not been well explained in theory. Moreover, empirical EoS methods may be inaccurate or even fail beyond the training conditions around the critical pressure and temperature of substance.

Therefore, in theory, Virial EoS was proposed to describe real-fluid effects by introducing Virial coefficients. Hirschfelder et al. [21] developed the Virial EoS by using the real-fluid partition function theory in statistical mechanics and reported the method of Virial coefficients calculation (Noted as the Virial method). Bird et al. [22] and Rowlinson [23] provided the dimensionless table of Virial coefficients for the Lennard-Jones (6–12) potential [24] and Stockmayer potential [25], respectively. Kallmann [26] calculated the real-fluid thermodynamic properties of H_2, O_2, N_2, H_2O, CO_2, etc. by using the Virial method. However, the non-linear behavior between the real-fluid corrections and pressures was not considered. Although the Virial EoS has been widely studied, it has not been applied in the real-fluid simulations with consistent computations of properties of substance, thermodynamics, transport, and reaction rates.

In this work, the Virial EoS method coupled with the real-gas partition function has been consistently used to describe real-fluid EoS, thermodynamic properties, and chemical potential calculations. The method is incorporated into Cantera software [19] to realize real-fluid simulations for the first time. The real-fluid impact on substance properties, thermodynamic properties, and chemical potentials has been respectively evaluated. This work also provides the comparisons between experimental data in literatures and simulation results employing the Virial method and empirical RK method. The virial method in this work will be incorporated in new version of Cantera program.

2. Methods

For ideal gases (IG), the EoS is simple as:

$$p\tilde{V} = RT \tag{2}$$

where p and T are pressure and temperature, $\tilde{V}$ is volume per mole, R is the ideal gas constant. However, for real fluids, intermolecular force, intermolecular potential energy, and molecular volume are not negligible. Virial EoS [21] has been found useful to combine the ideal behaviors and corrections of real-fluid behaviors:

$$\frac{p\tilde{V}}{RT} = 1 + \frac{B(T)}{\tilde{V}} + \frac{C(T)}{\tilde{V}^2} + \frac{D(T)}{\tilde{V}^3} + \cdots \tag{3}$$

The coefficients $B(T)$, $C(T)$, and $D(T)$ are called the second, third, and fourth Virial coefficients, respectively. These Virial coefficients represent corrections of real-fluid behaviors in the EoS. The expressions of Virial coefficients can be derived from real-fluid partition function calculations for different intermolecular potential models.

The EoS can be obtained from the partition function as:

$$p = \frac{RT}{\tilde{N}}\left(\frac{\partial \ln Z_N}{\partial V}\right)_T \tag{4}$$

$\tilde{N}$ is Avogadro constant. The partition function for a system of N molecules in classical statistics is given by:

$$Z_N = \frac{1}{N!h^{3N}} \iint e^{-\frac{H\left(\boldsymbol{r}^N,\ \boldsymbol{p}^N\right)\tilde{N}}{RT}} d\boldsymbol{r}^N d\boldsymbol{p}^N \tag{5}$$

in which the Hamiltonian $H(\boldsymbol{r}^N,\ \boldsymbol{p}^N)$ is given by:

$$H\left(\boldsymbol{r}^N,\ \boldsymbol{p}^N\right) = \sum_{i=1}^{N} \frac{{p_i}^2}{2m} + \Phi\left(\boldsymbol{r}^N\right) \tag{6}$$

h is Planck constant, $\boldsymbol{r}^N$and $\boldsymbol{p}^N$are position vector and momentum vector of molecules, m is molecular weight, $\Phi(\boldsymbol{r}^N)$ presents the intermolecular potential. Then we can obtain the EoS:

$$\begin{aligned} pV &= \frac{1}{N!h^{3N}Z_N} \iint e^{-H\left(\boldsymbol{r}^N,\ \boldsymbol{p}^N\right)/kT} \times \left[\frac{2}{3}\sum_{i=1}^{N}\frac{{p_i}^2}{2m} - \frac{1}{3}\sum_{i=1}^{N}\left(\boldsymbol{r}_i\frac{\partial}{\partial \boldsymbol{r}_i}\Phi\left(\boldsymbol{r}^N\right)\right)\right] \\ &\quad \times d\boldsymbol{r}^N d\boldsymbol{p}^N \\ &= NRT/\tilde{N} - \frac{1}{3(N-1)!\lambda^{3N}Z_N}\int^{W_N}\left(\boldsymbol{r}^N\right)\left(\boldsymbol{r}_i\frac{\partial}{\partial \boldsymbol{r}_i}\Phi\left(\boldsymbol{r}^N\right)\right)d\boldsymbol{r}^N \end{aligned} \tag{7}$$

in which $\lambda^2 = h^2/2\pi mkT$, $W_N(\boldsymbol{r}^N)$ is the Boltzmann factor:

$$W_N\left(\boldsymbol{r}^N\right) = e^{-\Phi\left(\boldsymbol{r}^N\right)\tilde{N}/RT} \tag{8}$$

In the second form of Eq. (7), the result shows explicitly the role of the intermolecular potential. Comparing Eqs. (3) and (7), the Virial coefficients can be computed from the real-fluid partition function based on different potential models. The Lennard-Jones (6–12) potential model [24]:

$$\varphi(r) = 4\epsilon\left[\left(\frac{\sigma}{r}\right)^{12} - \left(\frac{\sigma}{r}\right)^{6}\right] \tag{9}$$

has been widely employed for modeling the intermolecular collision of nonpolar molecules in gaseous and liquid states. ϵ and σ are force constants for the Lennard-Jones (6–12) potential. The Virial coefficients for nonpolar molecules in this work are obtained based on the Lennard-Jones (6–12) potential model.

The calculations of these Virial coefficients involve complex integrations. Bird et al. [22] calculated dimensionless Virial coefficients and their derivatives at different dimensionless temperatures as functions of ϵ and σ . The dimensionless temperature T^* is defined as:

$$T^* = \frac{RT}{\tilde{N}\epsilon} \tag{10}$$

The second Virial coefficient $B(T)$, dimensionless second Virial coefficient $B^\star(T^*)$ and its derivations $B_1^\star(T^*)$ and $B_2^\star(T^*)$ are defined as:

$$b_0 = \frac{2}{3}\pi\tilde{N}\sigma^3 \tag{11}$$

$$B(T) = b_0 B^\star(T^*) \tag{12}$$

$$B_1^\star(T^*) = T^*\left(\frac{dB^\star}{dT^*}\right) \tag{13}$$

$$B_2^\star(T^*) = T^{*2}\left(\frac{d^2B^\star}{dT^{*2}}\right) \tag{14}$$

b_0 is the volume of molecules.

For polar molecules, such as H_2O, CH_3OH and CH_3CHO, the Stockmayer potential model [25] has been widely used for Virial coefficients calculations:

$$\begin{aligned} \varphi(r,\ \theta_1,\ \theta_2,\ \phi_2-\phi_1) &= 4\epsilon\left[\left(\frac{\sigma}{r}\right)^{12} - \left(\frac{\sigma}{r}\right)^{6}\right] \\ &\quad - \frac{\mu^2}{r^3}g(\theta_1,\ \theta_2,\ \phi_2-\phi_1) \end{aligned} \tag{15}$$

The correction term $\frac{\mu^2}{r^3}g(\theta_1,\ \theta_2,\ \phi_2-\phi_1)$ is used to describe the mutual orientation of two polar molecules. The second Virial coefficient for the Stockmayer potential can be described as:

$$B(T) = b_0 B^{\star}(T^*;\ \mu^*) \tag{16}$$

It is noted that the dimensionless second Virial coefficient depends not only on dimensionless temperature T^* but also on dimensionless dipole moment $\mu^* = \mu/\sqrt{\epsilon\sigma^3}$ for polar molecules. Similar to nonpolar molecules, Rowlinson [23] calculated dimensionless Virial coefficients and their dimensionless derivatives at different dimensionless temperatures and dimensionless dipole moments for the Stockmayer potential model.

The corrections of the real-fluid thermodynamics functions from ideal values ($\tilde{H}-\tilde{H}^0$, $\tilde{S}-\tilde{S}^0$, $\tilde{C}_p-\tilde{C}_p^0$) can be calculated in terms of Virial coefficients [21]:

$$\frac{\tilde{H}-\tilde{H}^0}{RT} = T^*\left\{\frac{B^{\star}-B_1^{\star}}{V^{\star}} + \frac{C^{\star}-\frac{1}{2}C_1^{\star}}{(V^{\star})^2}+\cdots\right\} \tag{17}$$

$$\frac{\tilde{S}-\tilde{S}^0}{R} = -\left\{\frac{B_1^{\star}}{V^{\star}} + \frac{(B^{\star})^2-C^{\star}+C_1^{\star}}{2(V^{\star})^2}+\cdots\right\} \tag{18}$$

$$\frac{\tilde{C}_p-\tilde{C}_p^0}{R} = -\frac{B_2^{\star}}{V^{\star}} + \frac{(B^{\star}-B_1^{\star})^2-C^{\star}+C_1^{\star}+\frac{1}{2}C_2^{\star}}{(V^{\star})^2}+\cdots \tag{19}$$

where $V^{\star} = \tilde{V}/b_0$ is dimensionless volume.

The real-fluid behavior also has an impact on chemical potentials. Species activity is defined as a function of chemical potential μ_i for real fluids and μ_i^0 for ideal fluids [18]:

$$\alpha_i = exp\left(\frac{\mu_i-\mu_i^0}{RT}\right) \tag{20}$$

Activity coefficients γ_i is defined as:

$$\gamma_i = \frac{\alpha_i}{[X_i]/[X_i^0]} = \alpha_i\frac{pX_i/RT}{pX_i/ZRT} = Z\alpha_i$$

where X_i is molecular number of species i, $[X_i^0]$ and $[X_i]$ are the ideal- and real-fluid molar concentration, respectively. Z and γ_i are equal to 1 for ideal fluids. Therefore, γ_i can be derived as:

$$\gamma_i = Z\ exp\left(\frac{\mu_i-\mu_i^0}{RT}\right) \tag{21}$$

The rate of progress can be written as:

$$\dot{q} = k_f\prod C_{ac,i}^{\nu_i'} - k_r\prod C_{ac,i}{}^{\nu_i''} \tag{22}$$

where k_f and ν_i' are forward rate constants and stoichiometric constants of species i, while k_r and ν_i'' are reverse rate constants and stoichiometric constants of species i . $C_{ac,i}$ is the activity concentration of species i, which is functional with the correction of real-fluid chemical potential [18]:

$$C_{ac,i} = \gamma_i[X_i] = \frac{pX_i}{RT}exp\left(\frac{\mu_i-\mu_i^0}{RT}\right) \tag{23}$$

The corrections of chemical potential $\mu_i-\mu_i^0$ is relative to the correction of total Gibbs function:

$$\mu_i-\mu_i^0 = \left(\frac{\partial\left(n_T G - n_T G^0\right)}{\partial n_i}\right)_{T,V,n_{j\neq i}} \tag{24}$$

where n_T is the total number of molecules. According to the definition of Gibbs function ($G=H-TS$), $\mu_i-\mu_i^0$ is computed as:

$$\mu_i-\mu_i^0 = RT\frac{B_{mix}}{\tilde{V}} + 2RT\frac{1}{\tilde{V}}\left(\sum_j B_{ij}X_j - B_{mix}\right) \tag{25}$$

And then, $C_{ac,i}$ can be computed through Eqs. (23) and (25).

To describe real-fluid behaviors in fluid mixtures, a series of theoretical mixing rules [21] are applied for Virial coefficient calculations in this work. The second Virial coefficient B_{mix} in mixtures is obtained as:

$$B_{mix} = \sum_i\sum_j X_iX_jB_{ij} \tag{26}$$

Where X_i is mole fraction of ith species. The interactive second Virial coefficient B_{ij} is computed using corresponding interactive force constants σ_{ij} and ϵ_{ij}. For interactions between two non-polar molecules, species 1 and 2:

$$\sigma_{12} = \frac{1}{2}(\sigma_1+\sigma_2) \tag{27}$$

$$\epsilon_{12} = \sqrt{\epsilon_1\epsilon_2} \tag{28}$$

For interactions between two polar molecules, species 1 and 2:

$$\sigma_{12} = \frac{1}{2}(\sigma_1+\sigma_2) \tag{29}$$

$$\epsilon_{12} = \sqrt{\epsilon_1\epsilon_2} \tag{30}$$

$$\mu^* = \frac{\sqrt{\mu_1\mu_2}}{\sqrt{\epsilon_{12}\sigma_{12}{}^3}} \tag{31}$$

For interactions between a polar (p) and a non-polar (n) molecules:

$$\sigma_{np} = \frac{1}{2}(\sigma_n+\sigma_p)\xi^{-1/6} \tag{32}$$

$$\epsilon_{np} = \sqrt{\epsilon_n\epsilon_p}\ \xi^2 \tag{33}$$

$$\xi = \left[1+\frac{1}{4}\frac{\alpha_n\mu_p^{*2}}{\sigma_n{}^3}\sqrt{\frac{\epsilon_p}{\epsilon_n}}\right] \tag{34}$$

where α_n is the polarizability of the non-polar molecule. The corrections of volume, thermodynamics, and chemical potentials for fluid mixtures follow the same procedure of pure substance with applying the interactive virial coefficients and their derivatives.

All the equations above have been incorporated into Cantera Code [19] and packed as the Virial method to realize real-fluid simulations in this work. Flow reactor and ignition delay simulations for H_2 oxidation are performed by using 0-D homogenous module in Cantera. The Stanford hydrogen mechanism [27] is adopted in this work.

The RK EoS method is employed for comparison:

$$p = \frac{RT}{\tilde{V}-b} - \frac{a}{\tilde{V}\sqrt{T}\left(\tilde{V}+b\right)} \tag{35}$$

where a and b are parameters to describe intermolecular force and volume of molecules, respectively. These two parameters are computed by fitting critical temperatures, critical pressures, and their derivatives. The corrections of EoS, thermodynamic properties, and chemical potentials based on the RK method has been introduced in Cantera simulations by Kogekar et al. [18].

The Virial EoS method has several advantages comparing with RK EoS [12] and other similar empirical EoSs, such as SRK EoS [16] and PR EoS [17]. First, the Virial EoS is constructed with including intermolecular interactions and potentials by using real-fluid partition function theory in statistical mechanics. Therefore, the Virial coefficients in Virial EoS include deeper-level physical insights in real fluids compared to empirical parameters a and b in RK method. Second, Virial coefficients are functions of a broad

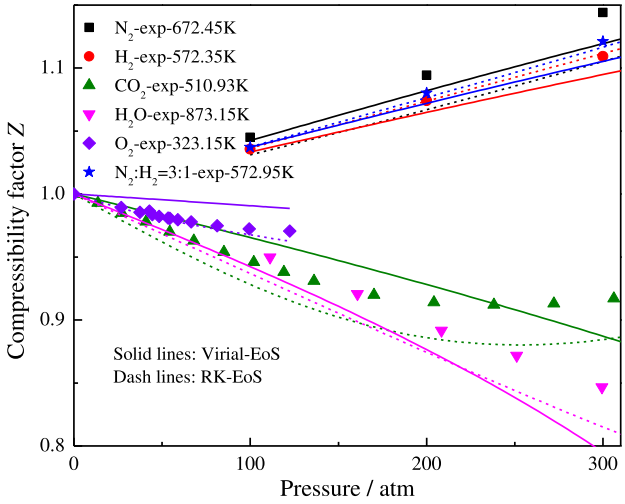

Fig. 1. The compressibility factors computed employing Virial EoS and RK EoS with comparison to experimental data of pure N_2 [29], H_2 [29], CO_2 [30], H_2O [31], O_2 [32] and mixture of N_2 and H_2 [29].

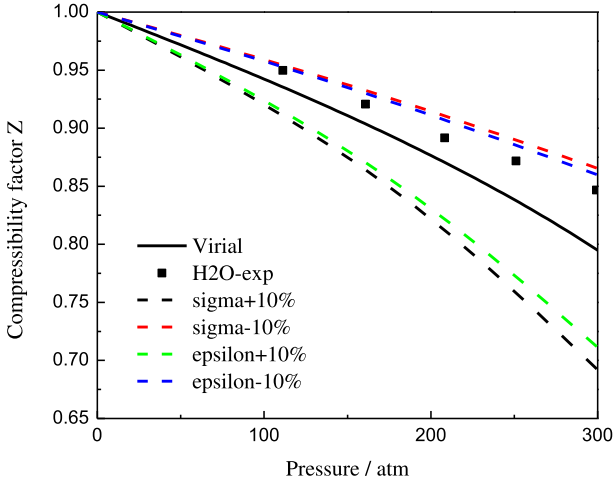

Fig. 2. The compressibility factors computed employing Virial EoS with comparison to experimental data of pure H_2O [31], parameters ϵ and σ are adjusted ± 10% from $\epsilon = 265.8\ \boldsymbol{cm}^{-1}$ and $\sigma = 2.648$ å [26] for test.

range of temperatures, while parameters a and b are fitted by using critical temperatures and critical pressures. It implies that the RK method may only be valid in the vicinity of critical temperatures and pressures, while the Virial method could keep accuracy in broader conditions. Third, from the physics of the Virial EoS, we could take more physical properties into consideration. For example, the polarizability of molecules was considered for the Virial coefficient calculations. Therefore, our corrections of EoS, thermodynamic properties, and chemical potentials could be more accurate. For example, the enthalpy and heat capacity of pure H_2O calculated using the Virial method at 100 atm are much closer to the data in JANAF table [28] than the RK method.

3. Result and discussion

3.1. Compressibility factor comparison

The compressibility factors computed by employing the Virial and RK methods are compared with experimental data in literatures [29–32] and are shown in Fig. 1. It shows that the compressibility factors calculated using Virial EoS possess good agreements with experimental data below 300 atm, especially for major dilute gases (N_2, CO_2 and H_2O). The good performance of compressibility factor calculations by using the RK method is because the EoS in the RK method is directly fitted based on critical temperatures and pressures, which corresponds to the compressibility factor calculations algebraically. Additionally, at higher pressures (above 300 atm), the Boltzmann assumption for diluted gas does not hold and the L-J potential is not accurate enough to describe intermolecular interactions. Therefore, the existing Virial method does not show privileges above 300 atm. With including non-Boltzmann distributions in the real-fluid partition function computation and more accurate intermolecular potential models, we believe the Virial method will still be more accurate than empirical methods above 300 atm. The development of the non-Boltzmann Virial method is our future work. The sensitivity test of parameters ϵ and σ on the compressibility factor of H_2O is shown in Fig. 2. The sensitivity test shows that the L-J potential parameters become more sensitive to the compressibility factor calculation with increasing pressures, which corresponds with the increasing real-fluid effect at higher pressures. Therefore, more accurate potential models should be employed at higher pressures and the non-Boltzmann interactions should also be considered. However, as the boundary condition has been fixed by applying critical pressures and temperatures in the RK method, no further physical consideration or adjustment can be added for improving real-fluid simulation at higher pressures. The L-J parameters used in this study are consistent with literature data [21,26].

3.2. Comparison for thermodynamic properties corrections

The calculation results of corrections of enthalpy (H), heat capacity (C_p), and entropy (S) at 1 atm for pure N_2 and H_2O and the comparison with U.S. Department of Energy RAND project [26] are shown in Table. S1 and S2 of Supplementary Document. The computation in the RAND project uses a similar Virial method. Our result show excellent agreements with the thermodynamic data in the RAND project.

Corrections of thermodynamic properties, such as enthalpy (H), heat capacity (C_p), and entropy (S), for pure H_2O at 100 atm are calculated using the Virial and the RK methods and are compared with the JANAF data [28] in Fig. 3. The JANAF data is obtained from the U.S. National Bureau of Standards (NBS) / National Research Council of Canada (NCR) steam tables developed by Harr et al. [33]. The data in NBS/NCR steam tables is obtained from the Helmholtz functions for H2O provided by Harr et al. The Helmholtz functions consist of 40 parameters and are fitted from plenty of experimental thermodynamic properties. Therefore, the thermodynamics data for H_2O in JANAF table is very reliable. In Fig. 3, the real-fluid corrections of enthalpy and heat capacity using the Virial method show better agreements with the JANAF data than using the RK method. And for entropy, the real-fluid correction of entropy using the RK method is not accessible because the RK code in Cantera does not involve the computation of entropy correction. However, we can still observe that the difference between the entropy corrections in the Virial method and in the JANAF table is insignificant. Compared with the ideal thermodynamic properties of H_2O ($H = -219.7$ kJ/mol, $C_p = 40.2$ J/mol/K, $S = 228.4$ J/mol/K at 900 K [34]), the real-fluid effect on heat capacity is significant at high pressures, which is about 10–20% larger than the ideal-gas value between 800 and 1000 K at 100 atm. Since heat capacity is crucial for temperature change in reactive systems, 10–20% deviation of heat capacity can cause considerable change of temperature and system reactivity in simulations, especially using H_2O and CO_2 as bath gases. Additionally, due to underestimation of real-fluid effects on heat capacity in the RK method, deeper weakness may appear in its adiabatic simulations.

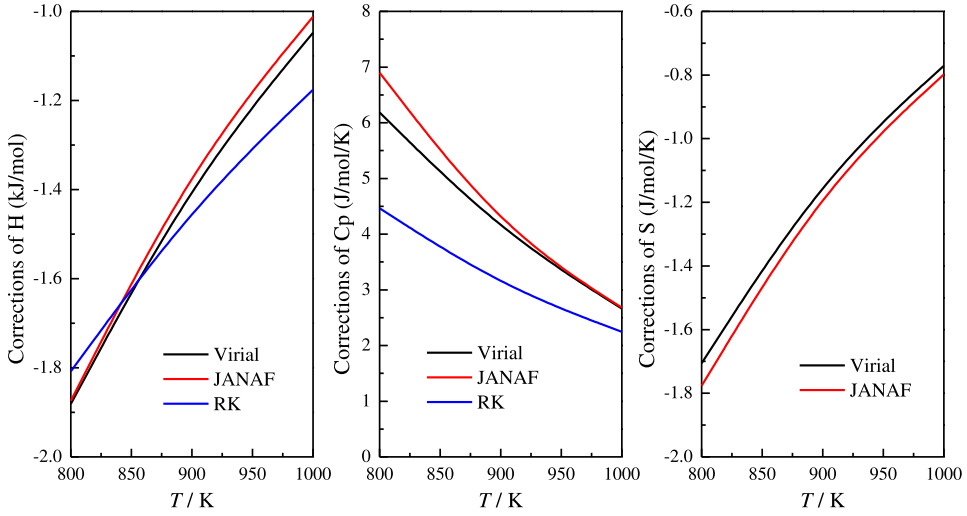

Fig. 3. Real-fluid corrections of thermodynamic properties enthalpy (H), heat capacity (C_p), and entropy (S) for pure H_2O at 100 atm calculated using the Virial and the RK methods and comparison with JANAF data [28].

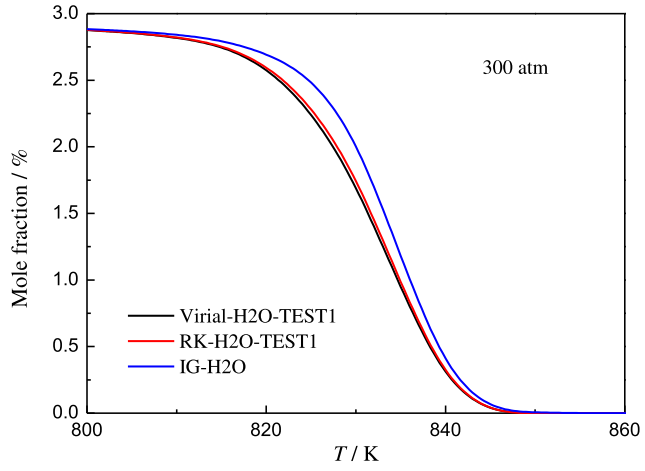

Fig. 4. Mole fraction of H_2 verse temperature at 300 atm in the adiabatic flow reactor simulation by using Virial-TEST1, RK-TEST1, and ideal-gas EoS. TEST1:real-fluid EoS only. H_2:O_2:H_2O = 2.9:4.24:92.86. Residence time = 295 K * 0.6 s / T.

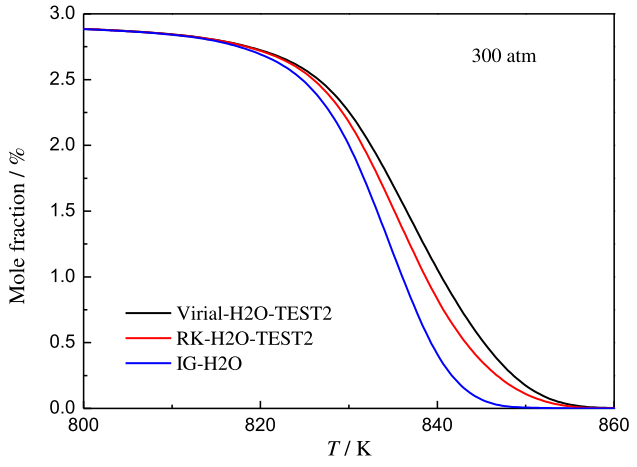

Fig. 5. Mole fraction of H_2 verse temperature at 300 atm in the adiabatic flow reactor simulation by using Virial-TEST2, RK-TEST2, and ideal-gas EoS. TEST2:real-fluid thermodynamic properties only. H_2:O_2:H_2O = 2.9:4.24:92.86. Residence time = 295 K * 0.6 s / T.

3.3. Simulation results of hydrogen oxidation

In order to investigate the effects of real-fluid EoS, real-fluid thermodynamic properties, and real-fluid chemical potentials on simulation separately, the Virial method is modified to three test codes, TEST1, TEST2, and TEST3. The three trials of H_2 oxidation are performed in the adiabatic flow reactor simulation using H_2O as bath gas at 300 atm, and are shown in Fig. 4 and Fig. 6, respectively. In Fig. 4, TEST1 only considers the influence of real-fluid EoS in simulations. In another word, we only change the calculation formula of molar volume by introducing compressibility factor, while employ the ideal-gas thermodynamic properties and chemical potentials. It is seen that real-fluid EoS promote the oxidation of hydrogen in the bath gas of H_2O because of the increase of density than the ideal-gas case. The predictions using Virial EoS and RK EoS are similar. However, real-fluid EoS inhibit the oxidation of hydrogen if the compressibility factor of bath gas is greater than 1 according to our tests, such as nitrogen, since real-fluid density becomes smaller. Mole fractions of H_2 verse temperature in N_2 diluent at 300 atm in the adiabatic flow reactor simulation by using Virial-TEST1, RK-TEST1, and ideal-gas EoS are shown in Fig. S1 of Supplementary Document.

In TEST2, we only consider the influence of real-fluid thermodynamic properties by introducing corrections of thermodynamics data while employing ideal-gas EoS and ideal-chemical potential computations. Based on our discussion in Fig. 3, the major impact of real-fluid thermodynamics comes from the increase of heat capacity, which results in a decrease of system temperature in the adiabatic simulation, so as to inhibit H_2 oxidation. The simulation using both Virial and RK method in Fig. 5 confirms the analysis above. The inhibition effect becomes more significant with faster hydrogen consumptions. The inhibition effects using the Virial method is stronger than using the RK method due to a larger corrective value of heat capacity in the Virial method. As is verified that the real-fluid heat capacity of H_2O is much more accurate using the Virial method in Fig. 3, the real-fluid modeling using the Virial method are more reliable, especially in adiabatic simulations. The influence of real-fluid heat capacity is similar in test of other bath gases.

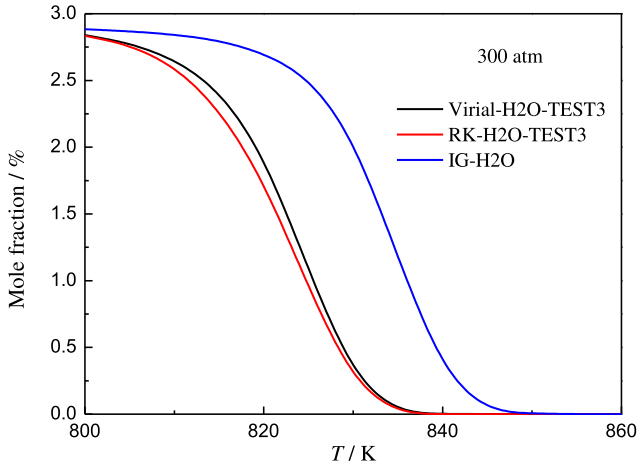

Fig. 6. Mole fraction of H_2 verse temperature at 300 atm in the adiabatic flow reactor simulation by using Virial EoS-TEST3, RK-TEST3, and ideal-gas EoS. TEST3: chemical potentials only. H_2:O_2:H_2O = 2.9:4.24:92.86. Residence time = 295 K * 0.6 s / T.

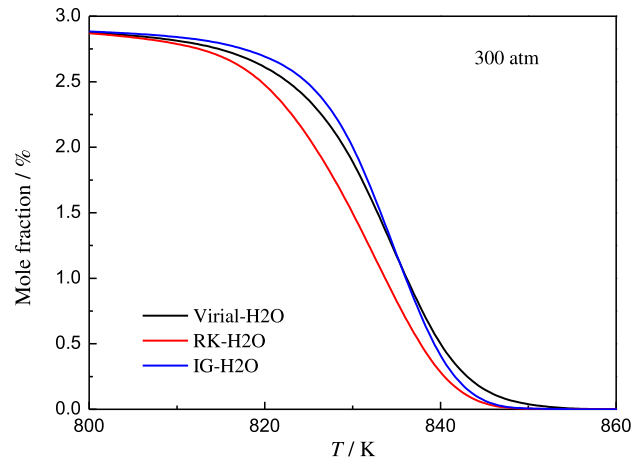

Fig. 7. Mole fraction of H_2 verse temperature at 300 atm in the adiabatic flow reactor simulation by using Virial, RK, and ideal-gas EoS. H_2:O_2:H_2O = 2.9:4.24:92.86. Residence time = 295 K * 0.6 s / T.

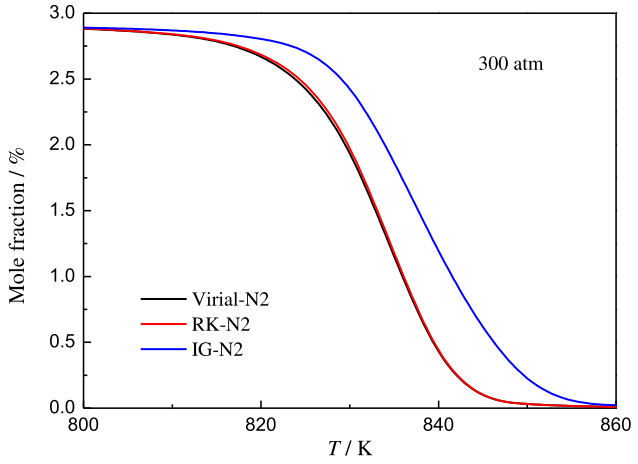

Fig. 8. Mole fraction of H_2 verse temperature at 300 atm in the adiabatic flow reactor simulation by using Virial, RK, and ideal-gas EoS. H_2:O_2:H_2O = 2.9:4.24:92.86. Residence time = 295 K * 0.6 s / T.

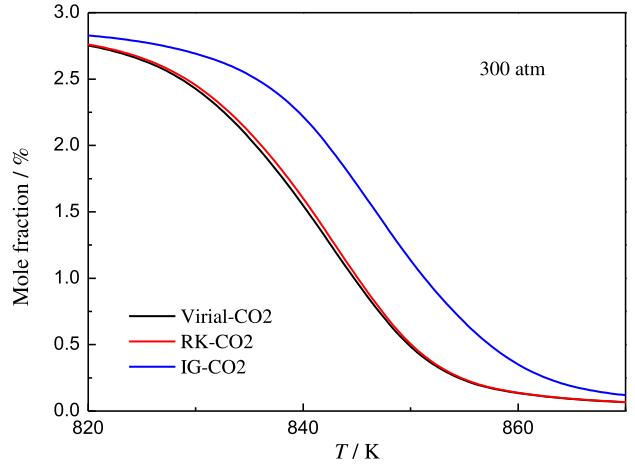

Fig. 9. Mole fraction of H_2 verse temperature at 300 atm in the adiabatic flow reactor simulation by using Virial, RK, and ideal-gas EoS. H_2:O_2:H_2O = 2.9:4.24:92.86. Residence time = 295 K * 0.6 s / T.

In TEST3, we only consider the influence of real-fluid chemical potentials in the Virial code. This correction increases species activity concentration s and then extensively accelerates reaction rates, which corresponds to the faster oxidation of hydrogen in the real-fluid simulation in Fig. 6. The predictions using the Virial and the RK method are similar. The influence of chemical potential is similar in test of other bath gases.

Combining these three parts of real-fluid effects, the complete adiabatic simulation of H_2 oxidation using H_2O as bath gas at 300 atm is plotted in Fig. 7. The simulation results show distinct difference between the Virial and RK methods. According to discussions above, the predictions using the Virial and RK methods are similar in TEST1. Hence, the prediction difference is mainly caused by real-fluid corrections of heat capacity and chemical potential of H_2O.

The speciation simulations for H_2 oxidation at 300 atm in adiabatic conditions using nitrogen and carbon dioxide as bath gases are respectively shown in Figs. 8 and **9**. It is seen that real-fluid behaviors overall promote the consumption of hydrogen in bath gases of both nitrogen and carbon dioxide. This is because the corrections of heat capacity in bath gases of nitrogen and carbon dioxide are insignificant. The effects of real-fluid EoS and chemical potentials are dominant and promote the consumption of hydrogen. The results calculated using the Virial and RK methods show good consistent for both two dilute gases.

The speciation simulations for H_2 oxidation at 300 atm under isothermal conditions using H_2O as bath gases are shown in Fig. 10. Since there are no temperature changes in isothermal conditions, the effects of real-fluid heat capacity are eliminated. Hence, the predictions show faster consumption of hydrogen with effects of real-fluid EoS and chemical potentials. The results calculated using the Virial and RK methods show insignificant difference.

The ignition delay time simulations for H_2 oxidation at 300 atm in H_2O are shown in Fig. 11. The ignition delay times are defined by the time at the maximum of the pressure gradient. Modeling using both real-fluid methods could reduce the ignition delay time up to 20% at 1150 K. The ignition delay time using the Virial method is longer than using the RK method because of larger heat capacity of H_2O in real fluid.

The modeling by using the Virial and RK methods also compared with experimental data of literatures in the present work. Comparisons of H_2 conversion in the isothermal flow reactor simulations with experimental data [35,36] in supercritical H_2O are shown in Fig. 12. Yetter et al. [37,38] and Li et al. [20] have re-

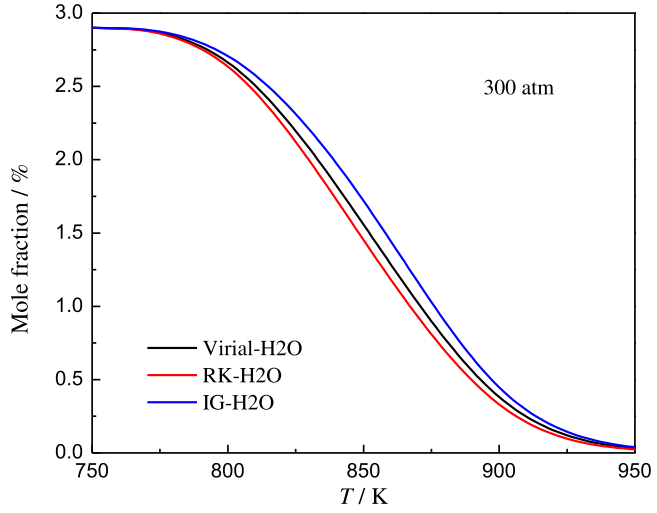

Fig. 10. Mole fraction of H_2 verse temperature at 300 atm in the isothermal flow reactor simulation by using Virial, RK, and ideal-gas EoS. H_2:O_2:H_2O = 2.9:4.24:92.86. Residence time = 295 K * 0.6 s / T.

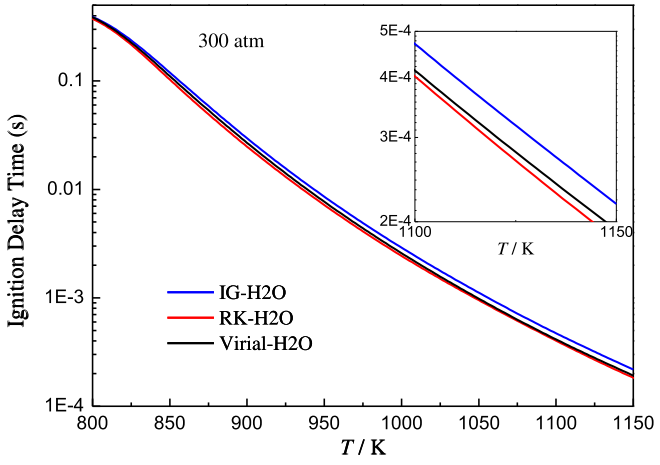

Fig. 11. The ignition delay time modeling for H_2 oxidation at 300 atm under constant-volume and adiabatic conditions using H_2O as bath gases. H_2:O_2:H_2O = 2.9:4.24:92.86.

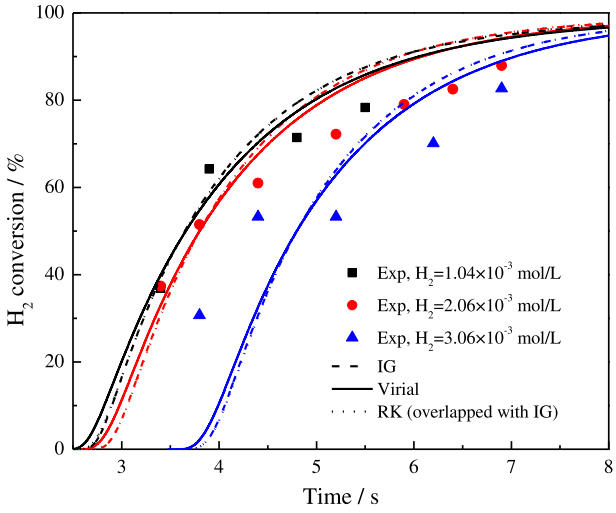

Fig. 12. The H_2 conversion verse time in the isothermal flow reactor simulations using the Virial, RK and ideal-gas methods and their comparisons with experimental data [35,36] in supercritical H_2O. T = 823.15 K, P = 24.6 MPa, and φ = 0.99. Modeling curves are shifted to match experimental data when 50% of H_2 conversion [37,38].

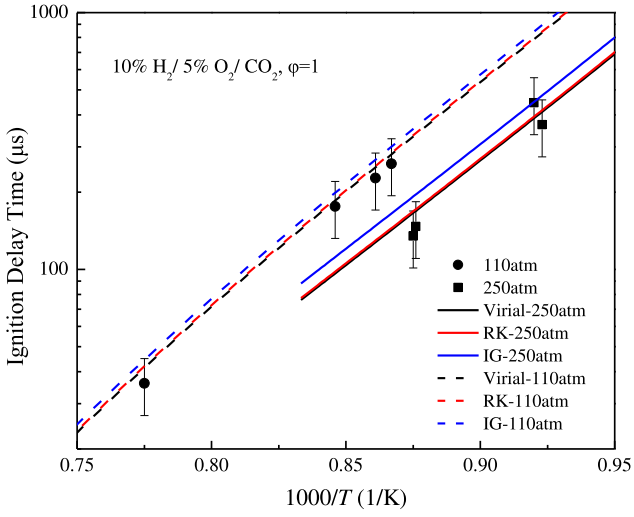

Fig. 13. The ignition delay time modeling for H_2 oxidation in carbon dioxide and comparison with experimental data [39].

ported the difficulties of modeling transient flow reactor experiment due to unknown induction time. They solve this problem by shifting simulation curves to match experimental data when 50% consumption of fuels occurs. Thus, a similar treatment is performed in our modeling. In Fig. 12, the modeling results using the RK method are almost overlapped with ideal gas curves since the shifting treatment covers up the effects of real-fluid behavior. However, the slope of modeling curves using the Virial method is smaller and closer to experimental data for all hydrogen concentrations than the RK method. The better performance of the Virial method is due to the more accurate prediction of heat capacity of H_2O.

Comparisons of ignition delay time modeling with experimental data in carbon dioxide [39] at high pressures are shown in Fig. 13. At both 110 and 250 atm, modeling results using both real-fluid methods show better agreement with experimental data. The similar performance of these two methods in CO_2 diluent in Fig. 13 corresponds the similar simulation results in Figs. 8 and 9.

According to the discussion above, as the Virial method has considered molecular polarization and shows higher accuracy of thermodynamic property calculations than the RK method, it is seen from Fig. 4. Fig. 9 that the Virial method gains additional modeling strength at adiabatic conditions in the bath gas of polar molecules like H_2O. Hence, we believe the Virial method can not only provide accurate estimations of real-fluid behavior at high pressures, but also provides physical insights in the intermolecular interactions under supercritical conditions.

Real-fluid effects on compressibility factors, thermodynamic properties, chemical potentials, transport properties, and rate constants and further on system reactivity are summarized in Fig. 14. It gives an overall view of influence of real fluid on reactive flow simulations. The impact of real-fluid EoS on system reactivity depends on the compressibility factor of bath gas, $Z > 1$ for nitrogen, $Z < 1$ for H_2O and carbon dioxide. Real-fluid effects on transport properties and rate constants still need further studies in the future.

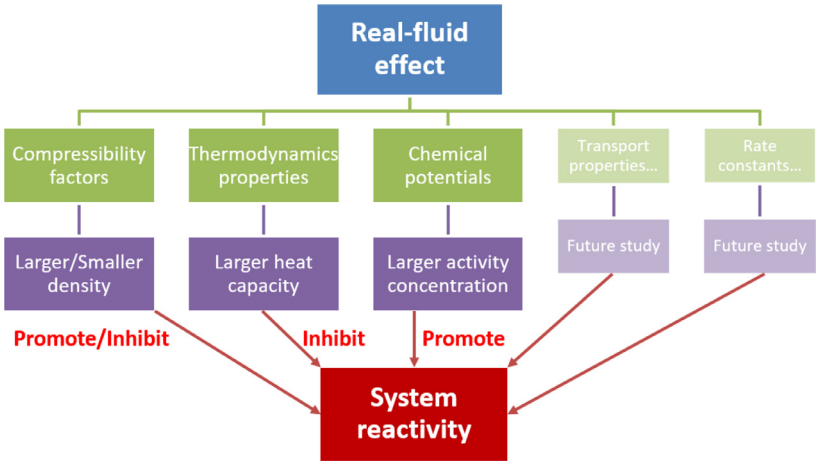

Fig. 14. Diagram of real-fluid effects on reactive flow simulations.

4. Conclusion

The Virial equation of state (EoS) method coupled with the real-fluid partition function theory has been consistently used to describe real-fluid EoS, thermodynamic properties, and chemical potential calculations. Different from conventional empirical Redlich-Kwong (RK) EoS, the Virial method is constructed with including intermolecular interactions, potentials, and molecular polarizations with deeper-level physical insights on real fluids. The Virial method is for the first time incorporated into Cantera software to realize real-fluid simulations.

The calculations of species compressibility factors and thermodynamic properties by using the Virial method show a better agreement with experimental data in literature than using the RK method. Especially, the calculated heat capacity of H_2O is 10–20% higher than the value in ideal-gas at 100 atm. The Virial method also possesses a better performance in predicting experimental H_2 ignition delay times and H_2 speciation profiles from literatures. The effects of real fluid through corrections of compressibility factors, thermodynamic properties, and chemical potentials on supercritical H_2 oxidation simulations in H_2O, N_2, and CO_2 diluents have been rigorously analyzed, respectively. Simply put, an increase of compressibility factor and heat capacity results in a slower oxidation, while an increase of species chemical potential promotes the fuel oxidation in real fluid. Moreover, the Virial method gains additional modeling strength at adiabatic conditions in the bath gas of polar molecules like H_2O, because it has considered molecular polarizations and shows higher accuracy of thermodynamic property calculations than the RK method. Hence, we believe the Virial method can not only provide accurate estimations of real-fluid behavior, but also provides physical insights in the intermolecular interactions under supercritical conditions.

Declaration of Competing Interest

We declare that we have no financial and personal relationships with other people or organizations that can inappropriately influence our work, there is no professional or other personal interest of any nature or kind in any product, service and/or company that could be construed as influencing the position presented in, or the review of, the manuscript entitled. Hao Zhao, College of Engineering, Peking University, 9/30/2021

Acknowledgments

This work was supported by the Seed Fund of College of Engineering in Peking University and the Department Earning Scheme of Hong Kong Polytechnic University.

Supplementary materials

Supplementary material associated with this article can be found, in the online version, at doi:10.1016/j.combustflame.2021.111945.

References

[1] M. Li, H. Wu, T. Zhang, B. Shen, Q. Zhang, Z. Li, A comprehensive review of pilot ignited high pressure direct injection natural gas engines: factors affecting combustion, emissions and performance, Renew. Sustain. Energy Rev. 119 (2020) 109653.
[2] S.M. Correa, A review of NO_x formation under gas-turbine combustion conditions, Combust. Sci. Technol. 87 (1993) 329–362.
[3] J.C. Oefelein, V. Yang, Modeling high-pressure mixing and combustion processes in liquid rocket engines, J. Propul. Power 14 (1998) 843–857.
[4] W. Liang, W. Li, C.K. Law, Laminar flame propagation in supercritical hydrogen/air and methane/air mixtures, Proc. Combust. Inst. 37 (2019) 1733–1739.
[5] M.P. Burke, M. Chaos, Y. Ju, F.L. Dryer, S.J. Klippenstein, Comprehensive H_2/O_2 kinetic model for high-pressure combustion, Int. J. Chem. Kinet. 44 (2012) 444–474.
[6] H. Zhao, C. Yan, T. Zhang, G. Ma, M.J. Souza, C.W. Zhou, Y. Ju, Studies of high--pressure n-butane oxidation with CO_2 dilution up to 100 atm using a supercritical-pressure jet-stirred reactor, Proc. Combust. Inst. 38 (2021) 279–287.
[7] N. Sakoda, K. Shindo, K. Shinzato, M. Kohno, Y. Takata, M. Fujii, Review of the thermodynamic properties of hydrogen based on existing equations of state, Int. J. Thermophys. 31 (2010) 276–296.
[8] R. Payri, F. Salvador, J. Gimeno, G. Bracho, The effect of temperature and pressure on thermodynamic properties of diesel and biodiesel fuels, Fuel 90 (2011) 1172–1180.
[9] A. Burcat, Thermochemical data for combustion calculations, Combustion Chemistry, Springer (1984), pp. 455–473.
[10] R.L. Scott, P.H. van Konynenburg, Static properties of solutions. Van der Waals and related models for hydrocarbon mixtures, Discuss. Faraday Soc. 49 (1970) 87–97.
[11] K.S. Pitzer, R. Curl Jr, The volumetric and thermodynamic properties of fluids.III. Empirical equation for the second virial coefficient, Molecular Structure And Statistical Thermodynamics: Selected Papers of Kenneth S Pitzer, World Scientific (1993), pp. 311–312.
[12] O. Redlich, J.N. Kwong, On the thermodynamics of solutions. V. An equation of state. Fugacities of gaseous solutions, Chem. Rev. 44 (1949) 233–244.
[13] F.H. MacDougall, On the dieterici equation of state, J. Am. Chem. Soc. 39 (1917) 1229–1235.
[14] J.A. Beattie, O.C. Bridgeman, A New Equation of State for Fluids, Proc. Am. Acad. Arts. Sci. 63 (1928) 229–308.
[15] M. Benedict, G.B. Webb, L.C. Rubin, An empirical equation for thermodynamic properties of light hydrocarbons and their mixtures II. Mixtures of methane, ethane, propane, and n-butane, J. Chem. Phys. 10 (1942) 747–758.

[16] G. Soave, Equilibrium constants from a modified Redlich-Kwong equation of state, Chem. Eng. Sci. 27 (1972) 1197–1203.
[17] D.Y. Peng, D.B. Robinson, A new two-constant equation of state, Ind. Eng. Chem. Fundam. 15 (1976) 59–64.
[18] G. Kogekar, C. Karakaya, G.J. Liskovich, M.A. Oehlschlaeger, S.C. DeCaluwe, R.J. Kee, Impact of non-ideal behavior on ignition delay and chemical kinetics in high-pressure shock tube reactors, Combust. Flame 189 (2018) 1–11.
[19] D.G. Goodwin, R.L. Speth, H.K. Moffat, B.W. Weber, Cantera: an object-oriented software toolkit for chemical kinetics, thermodynamics, and transport processes. https://www.cantera.org, 2018.
[20] G. Li, Y. Lu, P. Glarborg, Development of a detailed kinetic model for hydrogen oxidation in supercritical H_2O/CO_2 mixtures, Energy Fuels 34 (2020) 15379–15388.
[21] J.O. Hirschfelder, C.F. Curtiss, R.B. Bird, M.G. Mayer, Molecular theory of gases and liquids, Wiley, New York, 1964.
[22] R.B. Bird, E.L. Spotz, J. Hirschfelder, The third virial coefficient for non-polar gases, J. Chem. Phys. 18 (1950) 1395–1402.
[23] J. Rowlinson, The second virial coefficients of polar gases, Trans. Faraday Soc. 45 (1949) 974–984.
[24] J.E. Lennard-Jones, On the determination of molecular fields. II. From the equation of state of gas, Proc. R. Soc. A 106 (1924) 463–477.
[25] W.H. Stockmayer, Second virial coefficients of polar gases, J. Chem. Phys. 9 (1941) 398–402.
[26] H. Kallmann, Thermodynamic properties of real gases for use in high pressure problems, National Technical Information Service, 1950.
[27] Z. Hong, D.F. Davidson, R.K. Hanson, An improved H2/O2 mechanism based on recent shock tube/laser absorption measurements, Combust. Flame 158 (2011) 633–644.
[28] M. Chase, C. Davies, J. Downey, D. Frurip, R. McDonald, A. Syverud, NIST JANAF thermochemical tables version 1.0, US Department of Commerce, 1985.
[29] E.P. Bartlett, H. Cupples, T. Tremearne, The compressibility isotherms of hydrogen, nitrogen and a 3: 1 mixture of these gases at temperatures between 0 and 400 and at pressures to 1000 atmospheres, J. Am. Chem. Soc. 50 (1928) 1275–1288.
[30] H. Reamer, R. Olds, B. Sage, W. Lacey, Phase equilibrium in hydrocarbon systems. Methane–carbon dioxide system in the gaseous region, Ind. Eng. Chem. 36 (1944) 88–90.
[31] W. Kirillin, L. Rumjanzev, Experimental determination of the specific volume of steam from 92 to 524 atmospheres and from 430 to 600 C, Elektr. Stantsii 21 (1950) 8.
[32] A. Michels, H. Schamp, W. De Graaff, Compressibility isotherms of oxygen at 0°, 25° and 50°C and at pressures up to 135 atmospheres, Physica 20 (1954) 1209–1214.
[33] L. Harr, G. Kell, J. Gallagher, NBS/NCR steam tables, (1984).
[34] C.-.W. Zhou, Y. Li, U. Burke, C. Banyon, K.P. Somers, S. Ding, S. Khan, J.W. Hargis, T. Sikes, O. Mathieu, An experimental and chemical kinetic modeling study of 1, 3-butadiene combustion: ignition delay time and laminar flame speed measurements, Combust. Flame 197 (2018) 423–438.
[35] H.R. Holgate, J.W. Tester, Fundamental kinetics and mechanisms of hydrogen oxidation in supercritical water, Combust. Sci. Technol. 88 (1993) 369–397.
[36] H.R. Holgate, J.W. Tester, Oxidation of hydrogen and carbon monoxide in sub-and supercritical water: reaction kinetics, pathways, and water-density effects. 1. Experimental results, J. Phys. Chem. 98 (1994) 800–809.
[37] R.A. Yetter, F. Dryer, H. Rabitz, Flow reactor studies of carbon monoxide/hydrogen/oxygen kinetics, Combust. Sci. Technol. 79 (1991) 129–140.
[38] J. Roesler, R. Yetter, F.L. Dryer, Detailed kinetic modeling of moist CO oxidation inhibited by trace quantities of HCl, Combust. Sci. Technol. 85 (1992) 1–22.
[39] J. Shao, R. Choudhary, D.F. Davidson, R.K. Hanson, S. Barak, S. Vasu, Ignition delay times of methane and hydrogen highly diluted in carbon dioxide at high pressures up to 300 atm, Proc. Combust. Inst. 37 (2019) 4555–4562.